# Testing semilocal chiral two-nucleon interaction in selected electroweak processes

R. Skibiński, J. Golak, K. Topolnicki, and H. Witała

*M. Smoluchowski Institute of Physics, Jagiellonian University, PL-30348 Kraków, Poland*

E. Epelbaum and H. Krebs

*Institut für Theoretische Physik II, Ruhr-Universität Bochum, D-44780 Bochum, Germany*

H. Kamada

*Department of Physics, Faculty of Engineering, Kyushu Institute of Technology, Kitakyushu 804-8550, Japan*

Ulf-G. Meißner

*Helmholtz-Institut für Strahlen- und Kernphysik and Bethe Center for Theoretical Physics, Universität Bonn, D-53115 Bonn, Germany;*
*Institut für Kernphysik, Institute for Advanced Simulation and Jülich Center for Hadron Physics, Forschungszentrum Jülich,*
*D-52425 Jülich, Germany;*
*and JARA-High Performance Computing, Forschungszentrum Jülich, D-52425 Jülich, Germany*

A. Nogga

*Institut für Kernphysik, Institute for Advanced Simulation and Jülich Center for Hadron Physics, Forschungszentrum Jülich,*
*D-52425 Jülich, Germany*
*and JARA-High Performance Computing, Forschungszentrum Jülich, D-52425 Jülich, Germany*

The recently developed semilocal improved chiral nucleon-nucleon interaction is used for the first time to study several electromagnetic and weak processes at energies below the pion production threshold. Cross sections and selected polarization observables for deuteron photodisintegration, nucleon-deuteron radiative capture, three-body $^3$He photodisintegration, as well as capture rates for decays of the muonic $^2$H and $^3$He atoms are calculated. The Lippmann-Schwinger and Faddeev equations in momentum space are solved to obtain nuclear states. The electromagnetic current operator is taken as a single nucleon current supplemented by many-body contributions induced via the Siegert theorem. For muon capture processes the nonrelativistic weak current together with the dominant relativistic corrections is used. Our results compare well with experimental data, demonstrating the same quality as is observed for the semiphenomenological Argonne V18 potential. Compared to the older version of the chiral potential with a nonlocal regularization, a much smaller cut-off dependence is found for the state-of-art chiral local interaction employed in this paper. Finally, estimates of errors due to the truncation of the chiral expansion are given.

## I. INTRODUCTION

Studies of electromagnetic and weak reactions are an important part of nuclear physics. They deliver information on electromagnetic properties of nuclei, transitions between nuclear states and details of electromagnetic and weak currents inside nuclei [1–4]. In the broader sense the precise description of electromagnetic and weak reactions is a challenging test for models of the nuclear Hamiltonian and current operators as well as for the used theoretical schemes and numerical methods. Chiral effective field theory ($\chi$EFT) is currently the most important theoretical approach, which can and should be tested in investigations of electromagnetic and weak processes. Among many attempts to do that in the few-nucleon sector we mention Refs. [2,5,6] and references therein. However, these works were usually restricted to small energies or the lowest orders of the chiral expansion or combine the phenomenological potentials and chiral currents within the so-called "hybrid" $\chi$EFT approach or cover only selected reaction channels.

The continuous progress in the field of $\chi$EFT has resulted in the development of sophisticated nucleon-nucleon ($NN$) and many-nucleon interactions [7,8]. These forces have been used to describe reactions in three-nucleon ($3N$) systems [9–14], the structure of light nuclei [15], and nuclear matter [16]. Results obtained for $NN$ scattering at energies up to 300 MeV and nucleon-deuteron elastic scattering proved the usefulness and high quality of chiral potentials. In these first studies the regularization of $NN$ and $3N$ potentials in momentum space with the nonlocal regulator was used [17].

Recently it was shown [18,19] that such a regularization scheme introduces artifacts and affects the correct physical behavior of the potential at long distances. In addition, the spectral function regularization had to be introduced in order to cut off the unwanted short-range part of the two-pion exchange potential. This in turn causes too-strong dependence of predictions on values of the cut-off parameters [18,20]. The Bochum-Bonn group proposed recently in Refs. [21,22] an improved version of the chiral potential up to fifth order of the chiral expansion (N$^4$LO). During its construction,

regularization is performed in coordinate space and only afterwards such a regularized force is transformed to momentum space. In particular, the one-pion and the static two-pion exchange potentials are regularized in coordinate space by multiplying them by the function $f(\frac{r}{R}) = [1 - \exp(-(\frac{r}{R})^2]^6$, with $R$ being the cut-off (regularization) parameter. This procedure maintains the long-range part of the interaction and leads to smaller undesirable regularization effects. Indeed, as shown in Refs. [21,22] the $NN$ phase shifts as well as the deuteron properties are much less sensitive to the values of the regularization parameter $R$ than the ones obtained within the older version [17]. The same is also true for elastic nucleon-deuteron ($Nd$) scattering observables [23]. The three-nucleon force with consistent local regularization is under development, so in this paper we only use two-body interactions and, in addition, we neglect the Coulomb force.

One of the important and unique features of the $\chi$EFT approach is a possibility of a consistent derivation of nuclear forces and electroweak current operators, see, e.g., Refs. [24–28] for works in these directions. In particular, in Ref. [27] the long-range part of the leading two-pion exchange contributions was derived. Together with the well-known single nucleon current (SNC) and consistent old, nonlocal version of chiral interaction they were used to study the deuteron and the $^3$He photodisintegration in Refs. [29,30]. While the general description of observables was reasonable, a strong cut-off dependence of predictions was also observed. Similar results were obtained for radiative nucleon-deuteron capture and $^3$He photodisintegration where, instead of explicit many-body currents, the Siegert theorem was used [31]. The strong variation of predictions due to different values of the cut-off parameters practically precluded us from drawing detailed physical conclusions. Thus it is very interesting to see whether the cut-off dependence also becomes smaller for the electromagnetic processes, when the newly developed improved chiral interactions are considered. In the present work we use the Siegert approach and postpone studies based on explicit single-nucleon and many-body electromagnetic currents until a more complete picture of the electroweak current operator, consistent with the $NN$ interaction at each order of the chiral expansion, is known.

The question of the cut-off dependence can be also addressed in weak reactions. Thus we use the improved $NN$ forces [21,22] to calculate the capture rates in muon capture reactions on the deuteron and $^3$He. In this paper we employ a nonrelativistic single nucleon weak current operator supplemented with leading relativistic corrections (RC) [5,32,33]. Since we are mainly interested in the cut-off dependence of capture rates, the use of such an incomplete model of the current operator is justified in the present investigation.

The paper is organized as follows. In the next section we give a short overview of our formalism for electromagnetic and weak processes. Section III contains selected results for the deuteron photodisintegration process, $\gamma + d \rightarrow p + n$, while in Secs. IV and V we discuss $3N$ electromagnetic processes: nucleon-deuteron radiative capture, $n(p) + d \rightarrow \gamma + {}^3$H($^3$He), and the total $^3$He photodisintegration $\gamma + {}^3$He $\rightarrow p + p + n$, respectively. The results for weak muon capture

processes, $\mu^- + {}^2$H $\rightarrow n + n + \nu_\mu$, $\mu^- + {}^3$He $\rightarrow {}^3$H $+ \nu_\mu$, $\mu^- + {}^3$He $\rightarrow n + d + \nu_\mu$, and $\mu^- + {}^3$He $\rightarrow n + n + p + \nu_\mu$ are presented in Sec. VI. We summarize in Sec. VII.

## II. FORMALISM

The theoretical approach used in the present study is described in detail in Refs. [29,34–37], so here we only remind the reader of the key steps. We work in momentum space and employ a formalism based on the $3N$ Faddeev equations. The nuclear matrix elements for electromagnetic or weak disintegration processes are the central quantities from which we are able to calculate observables [33,36].

In the case of the deuteron photodisintegration, the nuclear matrix element $N_{deu}^\mu$ is defined as

$$N_{deu}^\mu \equiv \langle \Psi_{scatt}^{2N} | j_{2N}^\mu | \Psi_{bound}^{2N} \rangle, \qquad (2.1)$$

where $|\Psi_{scatt}^{2N}\rangle$ and $|\Psi_{bound}^{2N}\rangle$ are the final proton-neutron scattering state and the initial deuteron bound state, respectively. The deuteron state is a solution of the Schrödinger equation with the Hamiltonian comprising the $NN$ potential $V$. The same interaction, together with the free two-nucleon ($2N$) propagator $G_0$, enters the Lippmann-Schwinger equation for the $t$ operator, $t = V + tG_0V$, which we use to obtain the final scattering state. Then the $N_{deu}^\mu$ is given as

$$N_{deu}^\mu = \langle \vec{p}_0 | (1 + tG_0) j_{2N}^\mu | \Psi_{bound}^{2N} \rangle, \qquad (2.2)$$

where $|\vec{p}_0\rangle$ is the eigenstate of the relative proton-neutron momentum. The form of the electromagnetic current operator $j_{2N}^\mu$ is discussed below.

Radiative nucleon-deuteron capture is related via the time-reversal symmetry to the two-body $^3$He or $^3$H photodisintegration reactions. We exploit this relation and calculate the nuclear matrix element for the radiative Nd capture $N_{radNd}^\mu$ from the matrix element $N_{Nd}^\mu \equiv \langle \Psi_{scatt}^{Nd} | (1 + P) j_{3N}^\mu | \Psi_{bound}^{3N} \rangle$ for the photodisintegration reaction, leading to the final nucleon-deuteron scattering state $|\Psi_{scatt}^{Nd}\rangle$ [34,36]. The matrix element $N_{Nd}^\mu$ can be expressed as

$$N_{Nd}^\mu = \langle \phi_{Nd} | (1 + P) j_{3N}^\mu | \Psi_{bound}^{3N} \rangle + \langle \phi_{Nd} | P | U^\mu \rangle, \quad (2.3)$$

where $|\Psi_{bound}^{3N}\rangle$ is the $3N$ bound state while $|\phi_{Nd}\rangle$ is the product of the internal deuteron state and the state describing the free relative motion of the third nucleon with respect to the deuteron. $P = P_{12}P_{23} + P_{13}P_{23}$ is a permutation operator with $P_{ij}$ being the operator exchanging nucleons $i$ and $j$.

The auxiliary state $|U^\mu\rangle$ fulfills the Faddeev-like equation [36]

$$|U^\mu\rangle = tG_0(1 + P) j_{3N}^\mu | \Psi_{bound}^{3N} \rangle + tG_0P|U^\mu\rangle, \qquad (2.4)$$

with the free $3N$ propagator $G_0$.

The nuclear matrix element for $^3$He photodisintegration leading to three free nucleons in the final state, $N_{3N}^\mu \equiv \langle \Psi_{scatt}^{3N} | j_{3N}^\mu | \Psi_{bound}^{3N} \rangle$, is also given by the auxiliary state $|U^\mu\rangle$:

$$N_{3N}^\mu = \langle \Phi_{3N} | (1 + P) j_{3N}^\mu | \Psi_{bound}^{3N} \rangle + \langle \Phi_{3N} | (1 + P) | U^\mu \rangle,$$

$$(2.5)$$

where $|\Phi_{3N}\rangle$ is an antisymmetrized state describing the free motion of the three outgoing nucleons.

The nuclear electromagnetic current operators, $j_{2N}^\mu$ and $j_{3N}^\mu$, employed for the deuteron and $^3$He ($^3$H) photodisintegration processes, are constructed in the same way. Unfortunately, the $2N$ currents fully consistent with the locally regularized nuclear potentials are not yet available. Therefore, we approximate the electromagnetic current by a sum of contributions from the individual nucleons and supplement these results by the many-body parts incorporated via the Siegert theorem [34,36]. To this end we perform a multipole decomposition of the corresponding single nucleon current matrix elements and use standard identities [36] to express a part of the electric multipoles by the Coulomb multipoles, generated again by the single nucleon charge density operator. This step is justified by the fact that at low energies many-nucleon contributions to the nuclear charge density are small. The remaining part of the electric multipoles and all the magnetic multipoles are taken solely from the single nucleon current operators. The Siegert theorem, together with the so-called Siegert hypothesis, is also widely used in many calculations performed in coordinate space, see, e.g., Refs. [1,38–40]. This form of the nuclear current operator has the (purely technical) advantage that it does not depend on the nucleon-nucleon potential employed in our calculations. We denote this model of the current operator as SNC+Siegert.

The weak muon capture processes on atomic nuclei are described by means of similar nuclear matrix elements as in Eqs. (2.1)–(2.5), which are combined with the well-known leptonic part [41] to build the full transition amplitudes. Depending on the studied process the deuteron or $^3$He wave function represents the initial nuclear bound state. For the $\mu^- + {}^2\mathrm{H} \to n + n + \nu_\mu$ reaction, the final two-neutron scattering state is calculated using the $t$ operator. In the case of break-up channels in muon capture on $^3$He the corresponding two- and three-body scattering states are required. We calculate them analogously to the states for photodisintegration, again using Eq. (2.4), with the electromagnetic current $j_{3N}^\mu$ replaced by the weak current $j_w^\mu$ [5,32,33]. Since we solve Eq. (2.4) at a given energy of the $3N$ system, numerous solutions of Faddeev-like equation (2.4) have to be obtained in order to cover the whole range of the final muon neutrino energies. This significantly increases the numerical complexity of such calculations. Of course, in the case of the $\mu^- + {}^3\mathrm{He} \to {}^3\mathrm{H} + \nu_\mu$ channel we use only precalculated $^3$He and $^3$H states and no Faddeev equation for the bound state has to be solved repeatedly. For the weak current $j_w^\mu$ we employ a nonrelativistic single nucleon current operator supplemented by the dominant $(p/M_{\mathrm{nucl}})^2$ relativistic corrections, where $M_{\mathrm{nucl}}$ is the nucleon mass. A detailed discussion of the weak current, formulas connecting the nuclear matrix elements with the capture rates, and various aspects of the reaction kinematics are given in Ref. [33].

Our calculations are performed in momentum space and we use the formalism of partial waves. In the calculations we employ all partial waves in the two-body systems up to the two-body total angular momentum $j \leqslant 3$ and in the three-body states up to the three-body total angular momentum $J \leqslant \frac{15}{2}$. Such sets of partial waves guarantee convergence of predictions for all observables, see Refs. [36,42] for more technical details. The $3N$ bound states are obtained as in Ref. [43].

To estimate the theoretical errors of predictions arising from neglecting, at a given order of the chiral expansion, the contributions from higher orders, we apply the prescription given in Refs. [23,44]. Namely, we estimate the truncation error $\delta(X)^{(i)}$ of an observable $X$ at the $i$th order of the chiral expansion, with $i = 0,2,3,\dots$. If $Q$ denotes the chiral expansion parameter, then the expressions for truncation errors are

$$\delta(X)^{(0)} \geqslant \max(Q^2|X^{(0)}|, |X^{(i \geqslant 0)} - X^{(j \geqslant 0)}|),$$

$$\delta(X)^{(2)} = \max(Q^3|X^{(0)}|, Q|\Delta X^{(2)}|, |X^{(i \geqslant 2)} - X^{(j \geqslant 2)}|),$$

$$\delta(X)^{(i)} = \max(Q^{i+1}|X^{(0)}|, Q^{i-1}|\Delta X^{(2)}|, Q^{i-2}|\Delta X^{(3)}|)$$

$$\text{for } i \geqslant 3. \qquad (2.6)$$

In the above formulas $X^{(i)}$ is a prediction for the observable $X$ at $i$th order, $\Delta X^{(2)} \equiv X^{(2)} - X^{(0)}$, and $\Delta X^{(i)} \equiv X^{(i)} - X^{(i-1)}$ for $i \geqslant 3$. We also require that $\delta(X)^{(2)} \geqslant Q\delta(X)^{(0)}$ and $\delta(X)^{(i)} \geqslant Q\delta(X)^{(i-1)}$ for $i \geqslant 3$. In particular, such a way of theoretical error estimation takes into account the fact that our present calculations are incomplete as we do not include the $3N$ force starting from N$^2$LO. Furthermore, we do *not* estimate in this paper the uncertainty from the truncation of the chiral expansion of the current operators, which are included by means of the Siegert theorem at all considered orders. The actual theoretical uncertainty may, therefore, be larger than the values of $\delta(X)^{(i)}$ given below. A more reliable uncertainty quantification requires performing complete calculations including the corresponding $3N$ forces and exchange current operators. This work is in progress.

## III. RESULTS FOR DEUTERON PHOTODISINTEGRATION

In Fig. 1 we show the total cross section for the $\gamma + d \to n + p$ process at photon laboratory energies $E_\gamma$ up to 80 MeV obtained using the chiral $NN$ interaction at N$^4$LO [21,22] with the value of the regularization parameter $R = 0.9$ fm. In this
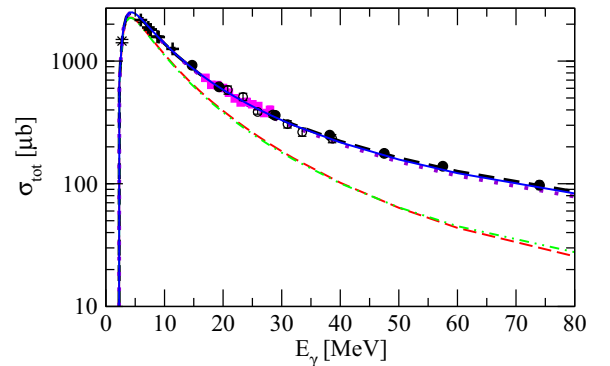


FIG. 1. The total cross section $\sigma_{\mathrm{tot}}$ for the $\gamma + d \to p + n$ reaction. The chiral N$^4$LO, $R = 0.9$ fm predictions for the SNC (SNC+Siegert) current model are shown with the dashed red (thick black dashed) curve. The AV18 predictions for the SNC, SNC+Siegert, and SNC+MEC current models are shown with the double-dotted-dashed green, dotted violet, and solid blue curves, respectively. The experimental data are from Ref. [46] (black "x"), [47] (magenta squares), [48] (open circles), [49] (black pluses), and [50] (black dots).
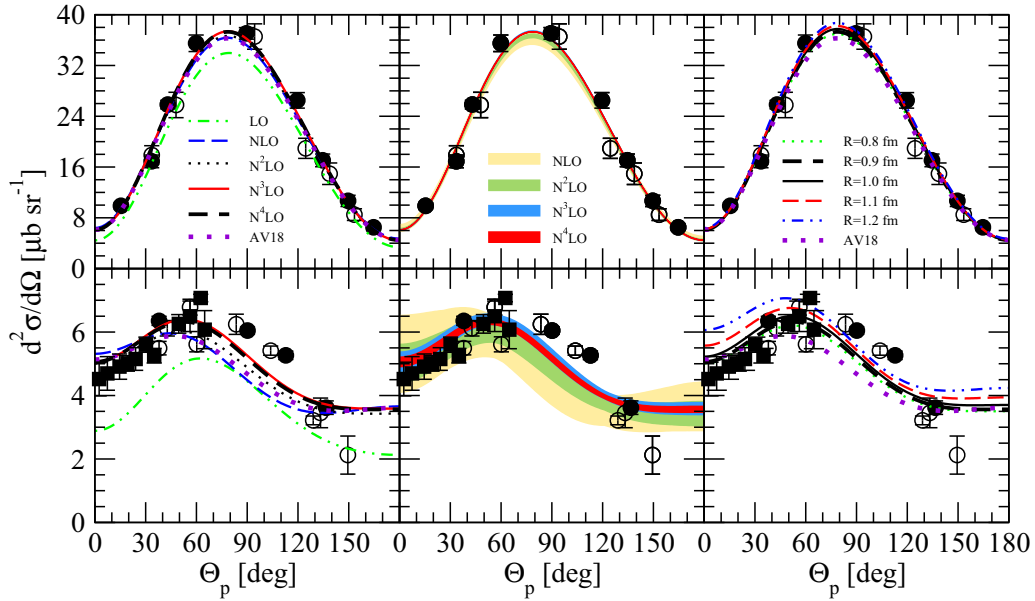
FIG. 2. The differential cross section $\frac{d^2\sigma}{d\Omega}$ for the $\gamma + d \rightarrow p + n$ reaction at $E_\gamma = 30$ MeV (the upper row) and $E_\gamma = 100$ MeV (the lower row) as a function of the proton center-of-mass scattering angle $\theta_p$. The left column shows the convergence of predictions at $R = 0.9$ fm with respect to the order of the chiral expansion (the double-dotted-dashed green, dashed blue, dotted black, solid red, and thick dashed black curves correspond to predictions at LO, NLO, N²LO, N³LO, and N⁴LO, respectively). The middle column shows the truncation errors (see text) at the different orders of the chiral expansion: NLO (yellow band), N²LO (green band), N³LO (turquoise band), and N⁴LO (red band). The right column shows the dependence of predictions at N⁴LO on the value of parameter $R$ (the dotted green, thick dashed black, solid black, dashed red, and double-dotted-dashed blue curves correspond to predictions with $R = 0.8, 0.9, 1.0, 1.1$, and $1.2$ fm, respectively). Note that the thick dashed black curve shown in both margin columns represents the same predictions. The thick violet dotted curve which represents the AV18 predictions is duplicated in the margin columns. All data points (open and solid circles and full squares) are from Ref. [51].

case we apply two models of the electromagnetic current: the SNC alone (the dashed red curve) and the SNC+Siegert (the thick dashed black curve). It is clear that while the omission of $2N$ currents leads to a poor description of the data, the SNC+Siegert approach yields an excellent agreement with the experimental results. For the sake of comparison with the predictions based on semiphenomenological forces, we show also predictions obtained with the Argonne V18 (AV18) $NN$ interaction [45] and three models of the nuclear current: SNC (green double-dotted-dashed curve), SNC+Siegert (dotted violet curve), and SNC+meson exchange currents (MEC) (blue solid curve). The SNC+MEC model comprises single nucleon contributions and the explicit $\pi$-like and $\rho$-like MEC linked to the AV18 $NN$ interaction (see Refs. [34,36] for more details). We observe that for this observable the implicit (SNC+Siegert) and explicit (SNC+MEC) ways of including many-body contributions to the current operator give quite similar predictions, which are in a very good agreement with the data, when the AV18 $NN$ potential is used to generate the $2N$ states. Further, the SNC+Siegert approach to the current operator works equally well with the chosen chiral and the AV18 $NN$ potentials. In both cases we obtain very similar predictions, practically indistinguishable at photon energies below approximately 30 MeV. At the higher energies a small difference develops between the chiral and the AV18 potential, with the chiral predictions lying closer to the data.

Next we study a more detailed observable, namely the differential cross section at two photon laboratory energies

$E_\gamma = 30$ MeV (Fig. 2, the upper row) and $E_\gamma = 100$ MeV (Fig. 2, the lower row). In the left panel we show the convergence of predictions for $R = 0.9$ fm with respect to the order of the chiral expansion. In the middle panel the uncertainty of theoretical predictions due to the truncation of higher-order contributions is given. Finally, in the right panel, we demonstrate the dependence of predictions on the values of the regulator $R$ at N⁴LO using five different values of $R$: 0.8, 0.9, 1.0, 1.1, and 1.2 fm. Our best prediction, SNC+Siegert for $R = 0.9$ fm is represented by the thick black dashed curve and is shown both in the left and right panels. For the sake of comparison, also the AV18 prediction given by the thick violet dotted line is displayed in these two panels. The same arrangement of curves will be preserved also in Figs. 3–6, 8, and 12.

It is clear that for both energies one has to go beyond the leading order (LO) to describe data. At the lower energy all the higher-than-LO predictions are close to each other, but at $E_\gamma = 100$ MeV the convergence is reached only at N³LO. The truncation errors presented in the central panel confirm this observation and the band at N⁴LO lies on the N³LO one. A small but visible width of the N⁴LO band for the higher energy suggests that some contributions from higher orders are still possible for this observable. The cut-off dependence of the cross section is very small at lower energy and increases with energy, reaching at $E_\gamma = 100$ MeV about 20% at small proton c.m. scattering angles. However, a more careful analysis reveals that predictions obtained with $R = 1.1$ fm and
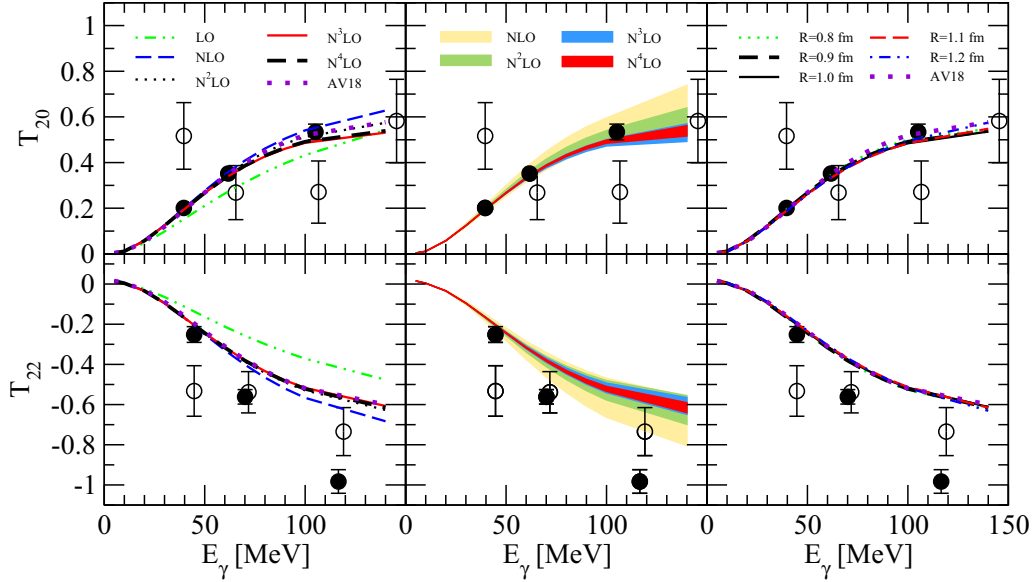
FIG. 3. The deuteron analyzing powers $T_{20}$ (top) and $T_{22}$ (bottom) for the $\gamma + d \rightarrow p + n$ reaction at $\Theta_p^{c.m.} = 88°$ and for $E_\gamma$ up to 150 MeV. The left column shows the convergence of predictions at $R = 0.9$ fm with respect to the order of the chiral expansion (curves as in Fig. 2). The middle column shows the truncation errors (see text) at different orders of the chiral expansion (bands as in Fig. 2). The right column shows the dependence of predictions at N$^4$LO on the value of the $R$ parameter (curves as in Fig. 2). The data are from Ref. [52] (filled circles) and Ref. [53] (open circles).

$R = 1.2$ fm are clearly far from the other ones, which are closer to each other. This observation is in agreement with the behavior of the cross section for the $NN$ and $Nd$ elastic scattering [23,44] and provide yet another indication that the theoretical uncertainty of the calculations using $R = 1.1$ fm and $R = 1.2$ fm is dominated by finite-regulator artifacts, see Ref. [21] for more details. Importantly, the cut-off dependence of the cross section observed here for the semilocal chiral force is much smaller than the cut-off dependence observed for the older version of the potential with the nonlocal regularization. As shown in Fig. 1 of Ref. [29] (pink band) for the older potential the cut-off dependence reaches 25% already at $E_\gamma = 30$ MeV and increases with photon energy. For the improved chiral force at N$^4$LO all predictions are slightly above the cross section calculated with the AV18 potential.

The data at $E_\gamma = 100$ MeV and at small angles between proton and photon momenta are better described by the AV18 force while data at bigger angles are closer to the chiral predictions.

We choose the deuteron tensor analyzing powers $T_{20}$ and $T_{22}$ as examples of polarization observables. Such observables are supposed to be more sensitive to the $NN$ interaction and the current operator used in the calculations. A measurement of these observables at proton scattering angle $\theta_p^{c.m.} = 88°$, where "c.m." denotes center of mass, has been reported in Ref. [52]. In Fig. 3 we compare our predictions for $T_{20}$ (top) and $T_{22}$ (bottom) with precise data from Ref. [52] and with older data from Ref. [53] for photon laboratory energies below $E_\gamma = 140$ MeV. The analyzing power $T_{20}$ is very well described by chiral predictions but for $T_{22}$ a clear discrepancy is seen with both sets of data above $E_\gamma = 50$ MeV.
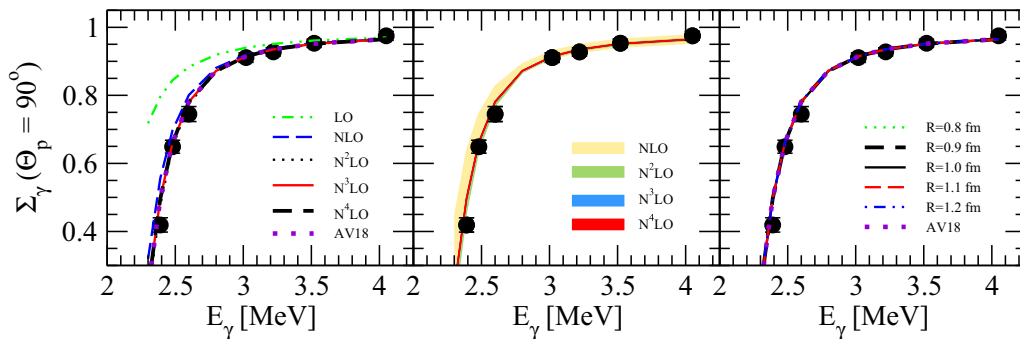


FIG. 4. The photon asymmetry $\Sigma_\gamma(\theta_p = 90°)$ at proton center-of-mass scattering angle $\theta_p = 90°$ for the $\gamma + d \rightarrow p + n$ reaction at low photon energies. The left column shows the convergence of predictions at $R = 0.9$ fm with respect to the order of the chiral expansion (curves as in Fig. 2). The middle column shows the truncation errors (see text) at the different orders of the chiral expansion (bands as in Fig. 2). The right column shows the dependence of predictions at N$^4$LO on the value of the $R$ parameter (curves as in Fig. 2 ). The data are from Ref. [55].
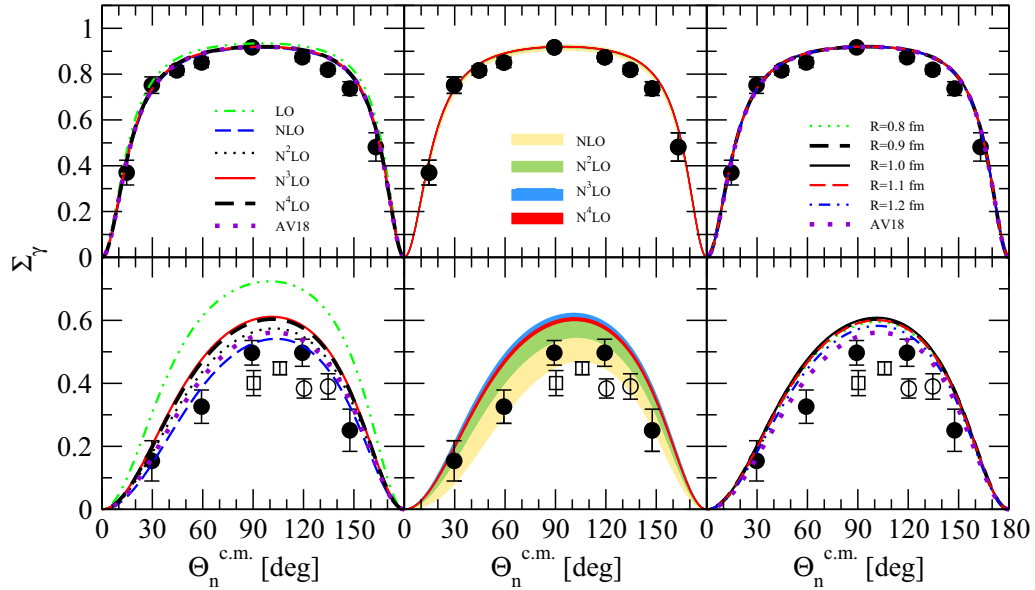
FIG. 5. The photon asymmetry $\Sigma_\gamma$ for the $\gamma + d \rightarrow p + n$ reaction at $E_\gamma = 19.8$ MeV (top) and 60.8 MeV (bottom) as a function of neutron center-of-mass scattering angle $\theta_n^{c.m.}$. The left column shows the convergence of predictions at $R = 0.9$ fm with respect to the order of the chiral expansion (curves as in Fig. 2). The middle column shows the truncation errors (see text) at the different orders of the chiral expansion (bands as in Fig. 2). The right column shows the dependence of predictions at N⁴LO on the value of the $R$ parameter (curves as in Fig. 2). The data are from Ref. [56] (filled circles), Ref. [57] (empty circles), and Ref. [58] (squares).

The predictions based on the chiral semilocal force show, for both analyzing powers, similar behaviour as for the differential unpolarized cross section—their convergence with respect to the chiral expansion, truncation errors, and cut-off dependence are very reasonable. Even for the highest energies the difference between N³LO and N⁴LO predictions is below 1.6% (1.3%) and the difference between predictions based on different values of the $R$ parameter does not exceed 7.3% (3.1%) for $T_{20}$ ($T_{22}$). Note that if we omit predictions with $R = 1.2$ fm, the latter numbers change to 2.3% (1.4%). The size of the truncation errors shows that only small contribution from higher orders can be expected even at energies above $E_\gamma = 50$ MeV.

It has been shown by Arenhövel and collaborators [52,54] in calculations with semi-phenomenological $NN$ forces that a more complete $2N$ current operator including, in addition to the implicit MEC (incorporated in the Siegert approach), also other explicit $2N$ operators, isobar configurations, and leading-order relativistic corrections leads to a much better description of $T_{22}$. Thus, the poor description of $T_{22}$ data in Fig. 3 can be attributed to the weaknesses of our model for the $2N$ electromagnetic current. This is interesting in view of future studies which will be performed with $NN$ interactions and current operators consistently derived within the $\chi$EFT framework. We would like to stress that such studies would benefit from precise measurements of the deuteron analyzing powers at energies below $E_\gamma = 140$ MeV in the whole range of scattering angles.

For the deuteron photodisintegration reaction also data for the photon asymmetry are available. In a recent precision experiment [55] the photon asymmetry $\Sigma_\gamma$ has been measured at the proton center-of-mass scattering angle $\theta = 90°$, for the

low photon laboratory energies up to 4.05 MeV. In Fig. 4 we compare our results with these data. As can be expected at such low energies, even predictions at lower orders are sufficient to describe the data. The results at N²LO, N³LO, and N⁴LO practically overlap. Also the predictions for different values of the $R$ regulator are very close to each other. The agreement with the data is excellent.

A precise measurement of the photon asymmetry in the $\gamma + d \rightarrow p + n$ reaction as a function of the neutron center-of-mass scattering angle at several photon energies has been reported in Ref. [56]. We choose two of them, $E_\gamma = 19.8$ MeV and 60.8 MeV, to give examples for small and medium photon energies. In Fig. 5 we compare our results with the data from Ref. [56] and Refs. [57,58]. At the lower photon energy we observe a similar picture as for the photon asymmetry $\Sigma_\gamma(\theta_p = 90°)$: Predictions are insensitive to the regulator value and to the order of the $NN$ interaction. Even predictions at LO describe data at $E_\gamma = 19.8$ MeV reasonably well. At $E_\gamma = 60.8$ MeV predictions for the photon asymmetry become convergent only at N³LO. The truncation errors and the range of predictions with the different values of the $R$ parameter at N⁴LO remain small. This again can be compared with predictions for the nonlocal force [17] shown in Ref. [29]. The improved interaction leads at $E_\gamma = 60.8$ MeV to a theoretical uncertainty approximately 2 times smaller than for the older force. The chiral predictions at the lower energy are in agreement with the data and are slightly above them at the higher energy. This may indicate that more sophisticated structures in the $2N$ current operator are required. The AV18 predictions are closer to the data but still overpredict them at the maximum of the photon asymmetry.
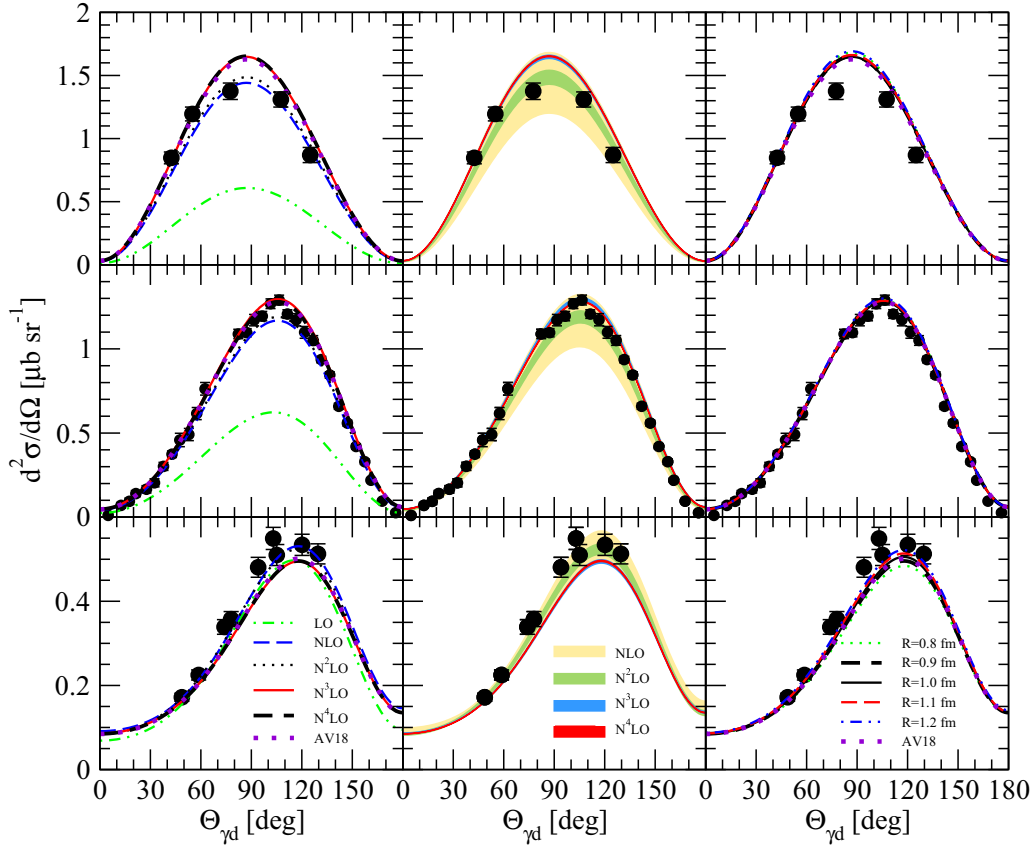
FIG. 6. The differential cross section $d^2\sigma/d\Omega$ for the $n + d \to {}^3\text{H} + \gamma$ reaction at $E_n = 9.0$ MeV (top) and for the $p + d \to {}^3\text{He} + \gamma$ reaction at $E_p = 29$ MeV (middle) and $E_p = 95$ MeV (bottom). The left column shows the convergence of predictions at $R = 0.9$ fm with respect to the order of the chiral expansion (curves as in Fig. 2). The middle column shows the truncation errors (see text) at the different orders of the chiral expansion (bands as in Fig. 2). The right column shows the dependence of the predictions at N$^4$LO on the value of the $R$ parameter (curves as in Fig. 2 ). The data at $E_n = 9.0$ MeV are from Ref. [59], at $E_p = 29$ MeV from Ref. [60], and at $E_p = 95$ MeV from Ref. [61].

## IV. RESULTS FOR NUCLEON-DEUTERON RADIATIVE CAPTURE

The three-nucleon systems pose another possibility to test models of nuclear dynamics. In Fig. 6 we show the differential cross section for the neutron-deuteron radiative capture reaction at the neutron laboratory energy $E_n = 9.0$ MeV (upper row) and for the proton-deuteron radiative capture at the proton laboratory energies $E_p = 29.0$ MeV (central row) and $E_p = 95.0$ MeV (lower row). For the neutron capture process the chiral predictions at next-to-leading order (NLO) and N$^2$LO agree with data but the N$^3$LO or N$^4$LO forces shift the predictions about 10% above the experimental points. It was shown in Ref. [31] that for the case of nonlocal regularization the $3N$ force reduces the cross section for this process at low energies also by about 10%. Thus it will be interesting to check
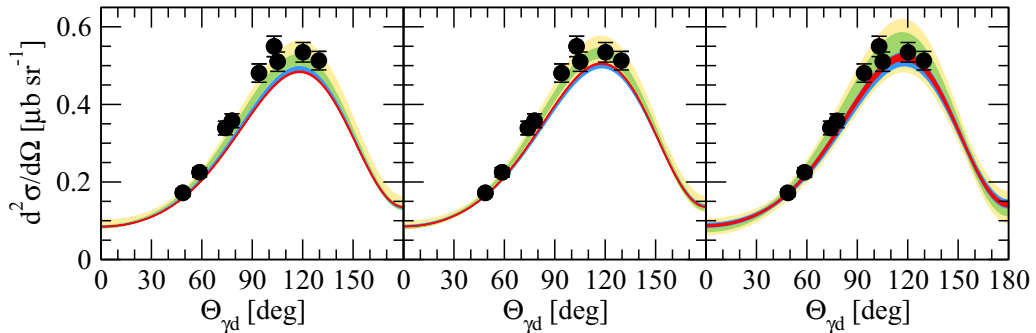


FIG. 7. The truncation errors at different orders of the chiral expansion for the same cross section as shown in Fig. 6 but at the proton energy $E_p = 95$ MeV only. The predictions have been obtained using the value of the regularization parameter $R = 0.8$ fm (left), $R = 1.0$ fm (middle), and $R = 1.2$ fm (right). Bands are as in Fig. 2 and data are from Ref. [61].
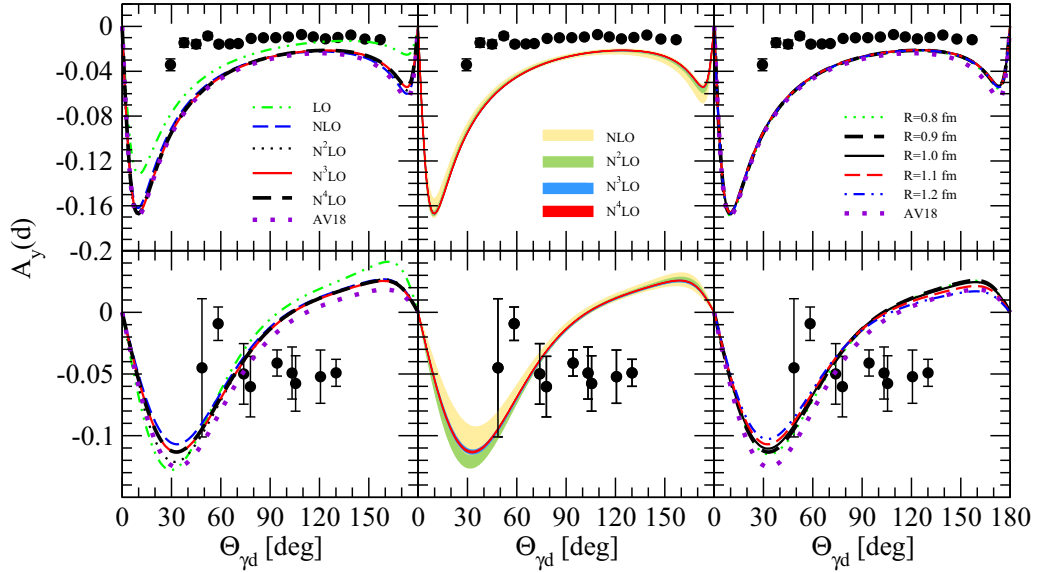
FIG. 8. The deuteron analyzing power $A_y(d)$ for the $p + d \rightarrow {}^3\text{He} + \gamma$ reaction at the deuteron laboratory energies $E_d = 17.5$ MeV (top) and $E_d = 95$ MeV (bottom). The left column shows the convergence of the predictions at $R = 0.9$ fm with respect to the order of the chiral expansion (curves as in Fig. 2). The middle column shows the truncation errors at the different orders of the chiral expansion (bands as in Fig. 2). The right column shows the dependence of predictions at N⁴LO on the value of the $R$ parameter (curves as in Fig. 2). The data at $E_p = 17.5$ MeV are from Refs. [62,63] and at $E_p = 95$ MeV from Ref. [61].

if the same is true for the locally regularized $3N$ force. The width of the band representing the truncation errors at N⁴LO is small and the cross section is practically independent from the choice of the regulator value.

In the case of the proton-deuteron radiative capture at presented here proton energies the $3N$ force effects (shown in Fig. 5 of Ref. [31]) differ. At $E_p = 29.0$ MeV they are small, so it is very likely that agreement of N⁴LO predictions
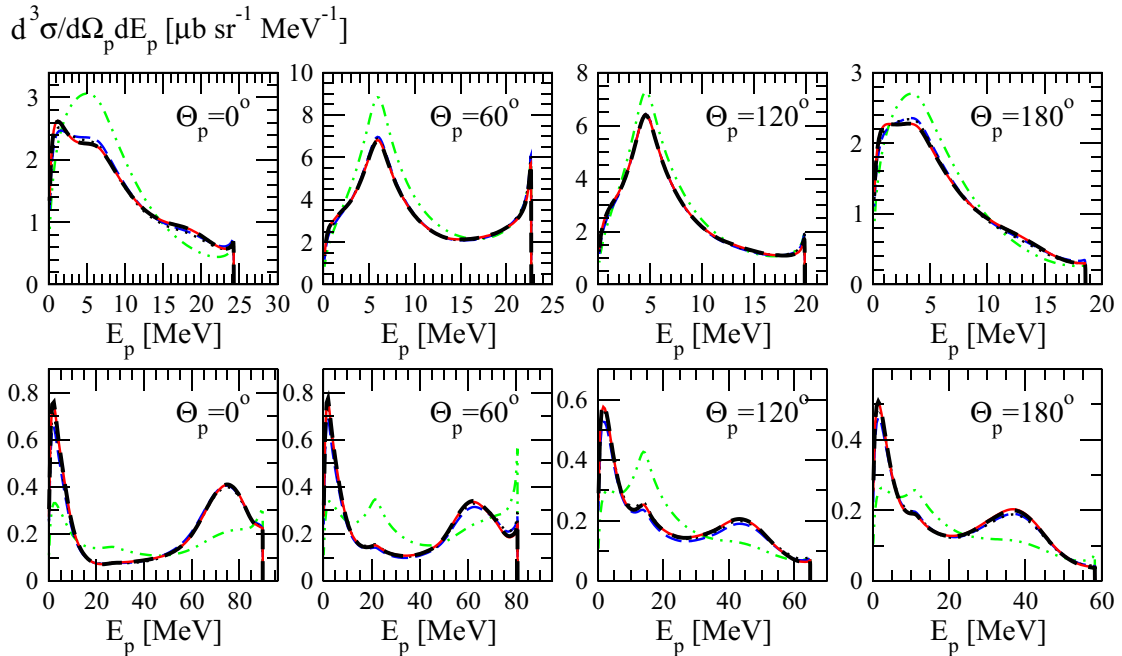


FIG. 9. The semi-inclusive ${}^3\text{He}(\gamma, p)pnpn$ cross section $\frac{d^3\sigma}{d\Omega_p dE_p}$ at $E_\gamma = 40$ MeV (top) and $E_\gamma = 120$ MeV (bottom) as a function of the outgoing proton energy $E_p$ for various angles $\Theta_p$ of the outgoing proton momentum with respect to the photon beam in the laboratory system. The predictions were obtained within the SNC+Siegert model and with the regulator $R = 0.9$ fm. The double-dotted-dashed green, dashed blue, dotted black, solid red, and thick dashed black curves correspond to LO, NLO, N²LO, N³LO, and N⁴LO predictions, respectively.

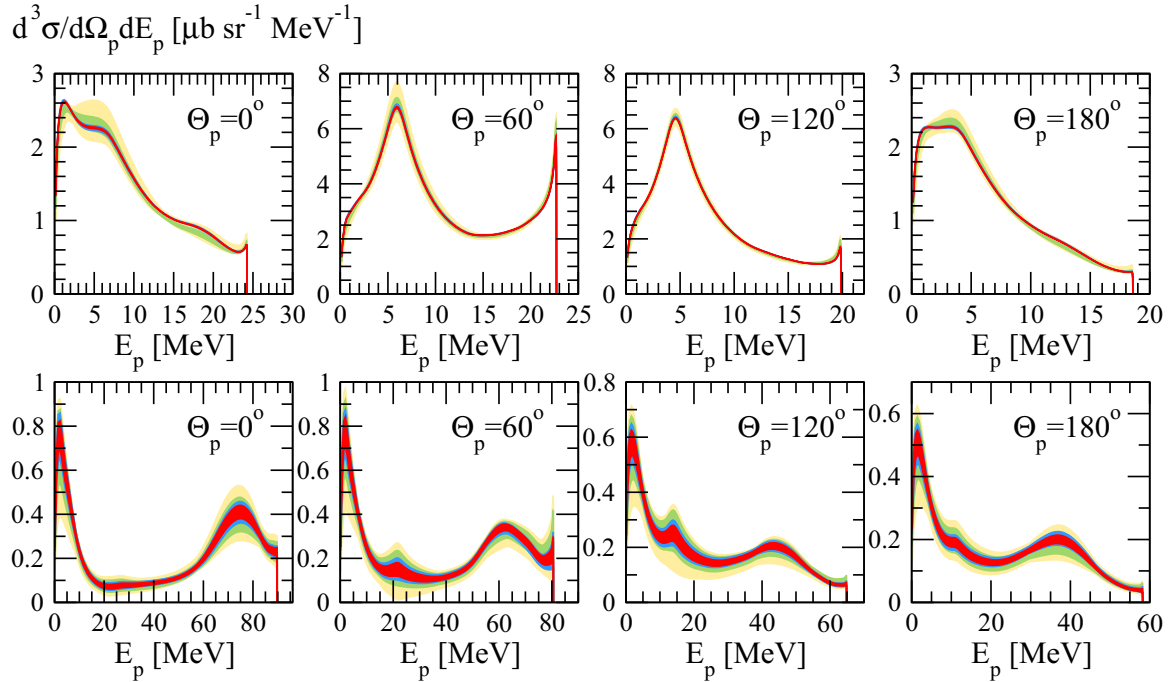$d^3\sigma/d\Omega_p dE_p$ [$\mu$b sr$^{-1}$ MeV$^{-1}$]



FIG. 10. The estimated higher-order truncation errors for the cross sections shown in Fig. 9. The yellow, green, turquoise, and red bands show the theoretical uncertainties at NLO, N$^2$LO, N$^3$LO, and N$^4$LO, respectively.

with the data, observed in Fig. 6, will remain if the locally regularized $3N$ force is included. At $E_p = 95$ MeV $3N$ force increases the cross section, so again it is possible that the observed underprediction of the cross section will be removed by the $3N$ interaction. It seems rather accidental that even at the highest energy the LO predictions are relatively

close to the other ones. The truncation errors and cut-off dependence remain small for both proton energies. This is very different from results obtained with explicit chiral MEC at LO and dominant terms at NLO for the old version of the potential with nonlocal regularization which show strong cut-off dependence—around 50% at $E_p = 50$ MeV (see Fig. 4

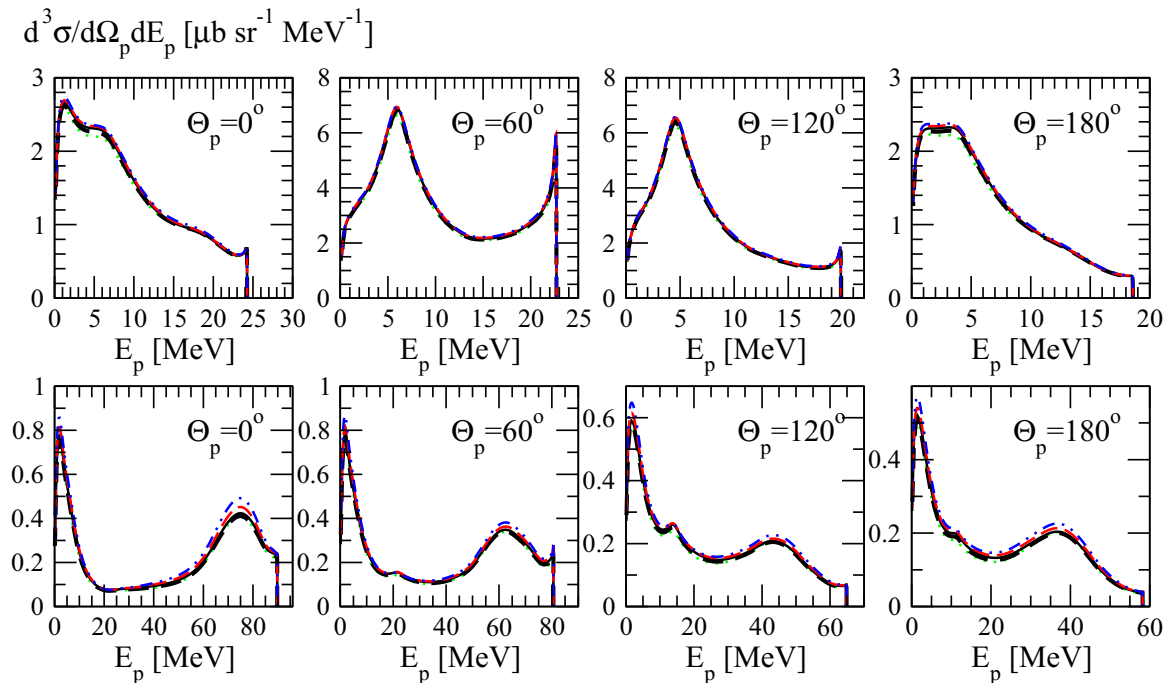$d^3\sigma/d\Omega_p dE_p$ [$\mu$b sr$^{-1}$ MeV$^{-1}$]



FIG. 11. The cut-off dependence of the cross sections shown in Fig. 9. The dotted green, thick dashed black, solid black, dashed red, and double-dotted-dashed blue curves are for $R = 0.8, 0.9, 1.0, 1.1, 1.2$ fm, respectively.
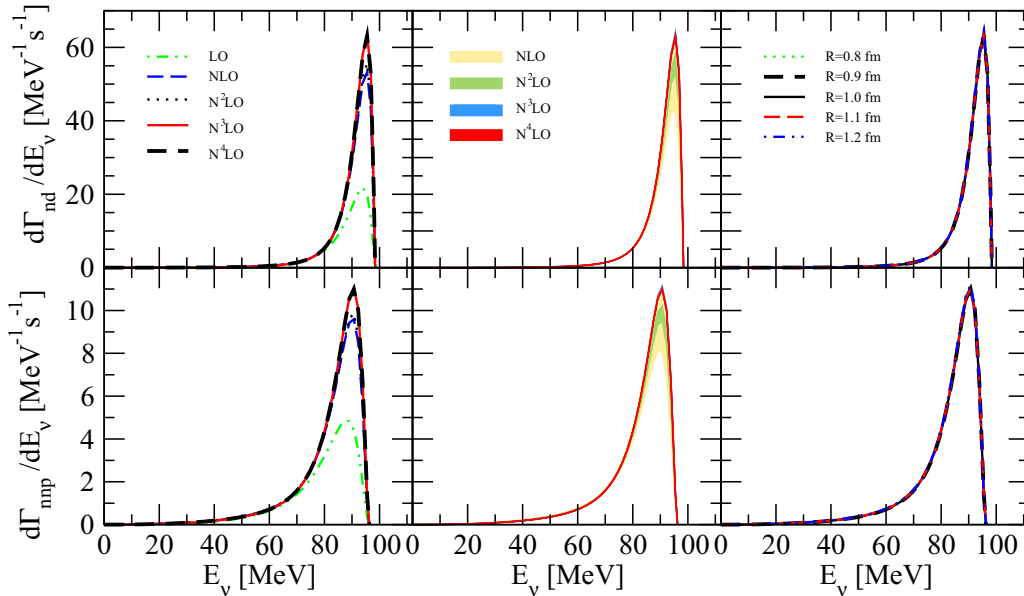
FIG. 12. The differential capture rates for two- and three-nucleon breakup channels: $\frac{d\Gamma_{nd}}{dE_\nu}$ (top) and $\frac{d\Gamma_{nnp}}{dE_\nu}$ (bottom) as a function of the outgoing neutrino energy $E_\nu$. The left column shows the convergence of predictions at $R = 0.9$ fm with respect to the chiral expansion order (curves for chiral predictions only as in Fig. 2). The middle column shows the truncation errors at the different orders of the chiral expansion (bands as in Fig. 2). The right column shows the dependence of predictions at N4LO on the value of the $R$ parameter (curves for chiral predictions only as in Fig. 2).

of Ref. [29]). However, one has to be careful comparing predictions from Ref. [29] with the current ones since it is expected that part of the cut-off dependence seen in Ref. [29] should be absorbed into short-range currents, neglected in Ref. [29]. Nevertheless, much smaller cut-off dependence and truncation errors observed with the local force [21,22] are very promising.

The size of the truncation errors clearly depends on the value of the regularization parameter $R$. In Fig. 7 we compare the truncation errors for the same differential cross section as shown in the last row of Fig. 6, i.e., at $E_p = 95$ MeV but for $R = 0.8$ fm (left), $R = 1.0$ fm (middle), and $R = 1.2$ fm (right). In all cases the truncation errors decrease with the growing chiral order and are very small at N4LO for $R = 0.8$ and 1.0 fm and much bigger for $R = 1.2$ fm. In particular, in the maximum of the cross section the bands width at N4LO are 0.003 $\mu$b/sr both for $R = 0.8$ and 1.0 fm and 0.017 $\mu$b/sr for $R = 1.2$ fm. The latter value is still approximately twice less than the spread of predictions at N4LO obtained with

different values of regularization parameter, which is $\Delta = 0.038$ $\mu$b/sr in the maximum of the cross section. This shows that fixing the value of regulator parameter is important for the analysis of theoretical uncertainties. In Refs. [21,22] the values of regularization parameter $R = 0.9$ fm and $R = 1.0$ fm have been recommended due to the best description of the nucleon-nucleon scattering data. Our findings on truncation errors also support this choice.

As an example of a polarization observable we choose the deuteron vector analyzing power $A_Y$ and show it in Fig. 8 at two deuteron laboratory energies $E_d = 17.5$ MeV (top) and $E_d = 95$ MeV (bottom). For both energies we observe nice behavior at orders above N2LO—the convergence with respect to chiral order is very good and truncation errors are diminishing. Also the cut-off dependence is negligible. That is a significant improvement when compared to the case of the nonlocal regularization [31]. At both energies the data description is poor; however, this observable depends strongly on the details of the nuclear current operator [34].

TABLE I. The doublet capture rates $\Gamma_d$ in $(s^{-1})$ for the $\mu^- + d \rightarrow n + n + \nu_\mu$ process obtained within the $NN$ interaction at given order and the SNC+RC model of the nuclear weak current operator (see text). In the next-to-last column the truncation error $\delta(\Gamma_d)$ at given order of the chiral expansion for the doublet capture rate, obtained for $R = 0.9$ fm, is given. In the last column the spread of the results at a given chiral order due to the different $R$ values, $\Delta$ in $(s^{-1})$, is shown.

| Chiral order | $R = 0.8$ fm | $R = 0.9$ fm | $R = 1.0$ fm | $R = 1.1$ fm | $R = 1.2$ fm | $\delta(\Gamma_d)$ | $\Delta$ |
|---|---|---|---|---|---|---|---|
| LO | 396.0 | 397.4 | 398.4 | 398.9 | 399.2 | 21.02 | 3.2 |
| NLO | 384.2 | 385.8 | 387.2 | 388.6 | 389.8 | 4.84 | 5.6 |
| N2LO | 385.0 | 386.1 | 387.2 | 388.3 | 389.3 | 1.11 | 4.3 |
| N3LO | 386.8 | 386.4 | 385.2 | 384.3 | 383.2 | 0.26 | 3.6 |
| N4LO | 385.5 | 386.1 | 386.3 | 385.6 | 384.6 | 0.06 | 1.7 |

TABLE II. The total capture rates $\Gamma$ in (s$^{-1}$) for the $\mu^- + {}^3\text{He} \rightarrow {}^3\text{H} + \nu_\mu$ process obtained within the $NN$ interaction at given order and the SNC+RC model of the nuclear weak current operator (see text). In the next-to-last column the truncation error $\delta(\Gamma)$ at the $i$th order of the chiral expansion for the total capture rate, obtained for $R = 0.9$ fm, is given. In the last column the spread of the results at a given chiral order due to the different $R$ values, $\Delta$ in (s$^{-1}$), is shown.

| Chiral order | $R = 0.8$ fm | $R = 0.9$ fm | $R = 1.0$ fm | $R = 1.1$ fm | $R = 1.2$ fm | $\delta(\Gamma)$ | $\Delta$ |
|---|---|---|---|---|---|---|---|
| LO | 1610 | 1618 | 1610 | 1594 | 1572 | 314.0 | 46 |
| NLO | 1330 | 1357 | 1381 | 1405 | 1427 | 72.2 | 97 |
| N$^2$LO | 1337 | 1356 | 1376 | 1395 | 1415 | 16.6 | 78 |
| N$^3$LO | 1314 | 1304 | 1289 | 1278 | 1266 | 3.8 | 48 |
| N$^4$LO | 1296 | 1307 | 1308 | 1299 | 1285 | 0.9 | 23 |

## V. THREE-BODY $^3$He PHOTODISINTEGRATION

We choose the semi-inclusive cross section $\frac{d^3\sigma}{d\Omega_p dE_p}$ as an example of an observable for three-body $^3$He photodisintegration. In this process only one of the three outgoing nucleons is detected and we assume that it is a proton. For this observable we have prepared three different Figs. 9–11, showing the dependence on the chiral order, error estimates, and the dependence on the regulator value at N$^4$LO. In all three figures we show the cross section at photon laboratory energy $E_\gamma = 40$ MeV and 120 MeV as a function of the final proton energy for the proton emerging at four angles $\Theta_p$ with respect to the photon beam: $\Theta_p = 0°, 60°, 120°,$ and $180°$. Since we focus here on predictions of the new local chiral potential, we refer the reader to Refs. [64] and [36] for the discussion on the origin of structures observed in the spectra.

In Fig. 9 we show the convergence of predictions with respect to the order of the chiral expansion for the detected proton at $E_\gamma = 40$ MeV (top) and $E_\gamma = 120$ MeV (bottom). Only predictions at LO are far from the rest and are surely not sufficient to describe the data. The other predictions are close to each other and, in particular, the N$^3$LO and N$^4$LO results practically overlap.

The bands giving the truncation errors for the semi-inclusive cross section are shown in Fig. 10. At the photon laboratory energy $E_\gamma = 40$ MeV a big contribution from higher orders is expected at the NLO (the yellow band) and still noticeable addition is expected at N$^2$LO (the green band). At higher orders bands are very narrow and they practically overlap. Thus one can conclude that for the presented here cross section, calculations at N$^3$LO should be sufficient. At the higher photon laboratory energy $E_\gamma = 120$ MeV the magnitude of the truncation errors is sizable even at N$^4$LO.

Finally, in Fig. 11 we explicitly show the dependence of the cross section on the value of the parameter $R$ used to regularize the chiral forces at N$^4$LO. The cut-off dependence at $E_\gamma = 40$ MeV is weak and its size is comparable with the truncation errors. At the higher energy clear differences between predictions based on different values of $R$ are seen. The range of predictions due to the different values of $R$ usually slightly exceeds the theoretical uncertainties at N$^4$LO shown in Fig. 10. Note, however, that the values $R = 0.9$ fm and $R = 1.0$ fm are preferred [21,22].

## VI. MUON CAPTURE

For the muonic deuterium atom the weak capture process leads to two neutrons and a muon neutrino in the final state. The total capture rates $\Gamma_d$ for this process are given in Table I. We also give the truncation error $\delta(\Gamma_d)^{(i)}$ [Eq. (2.6)] at a given order for $R = 0.9$ fm (the next-to-last column) and the maximal difference between predictions with different values of the regulator $R$ at a given order, $\Delta$ (the last column). We applied the SNC+RC model of the current operator and used values of the regularization parameter $R$ in the range from 0.8 to 1.2 fm. The truncation errors decreases significantly with the increasing order of the chiral expansion, confirming nice convergence of capture rate. At N$^4$LO and $R = 0.9$ fm $\delta(\Gamma_d)^{(5)}$ is about 0.02%. The truncation errors for $R = 1.2$ fm (not shown in the table) are much bigger, reaching 0.18% at N$^4$LO. The cut-off dependence is also weak, at N$^4$LO $\Delta = 1.7$ s$^{-1}$ what amounts to about 0.44% of the capture rate at $R = 0.9$ fm. The new predictions are also in agreement with the result based on the AV18 $NN$ force, which for the same model of the weak current is 382.3 s$^{-1}$.

In the case of muon capture on $^3$He three different final states are possible. First, the capture process can lead to the non-break-up channel with the final $^3$H nucleus and the

TABLE III. The same as in the Table II but for the $\mu^- + {}^3\text{He} \rightarrow d + n + \nu_\mu$ process.

| Chiral order | $R = 0.8$ fm | $R = 0.9$ fm | $R = 1.0$ fm | $R = 1.1$ fm | $R = 1.2$ fm | $\delta(\Gamma)$ | $\Delta$ |
|---|---|---|---|---|---|---|---|
| LO | 262 | 282 | 312 | 350 | 392 | 304.0 | 130 |
| NLO | 536 | 525 | 515 | 504 | 492 | 69.9 | 44 |
| N$^2$LO | 547 | 539 | 529 | 518 | 507 | 16.1 | 40 |
| N$^3$LO | 584 | 586 | 592 | 596 | 603 | 3.7 | 19 |
| N$^4$LO | 590 | 584 | 583 | 587 | 595 | 0.9 | 12 |

TABLE IV. The same as in the Table II but for the $\mu^- + {}^3\text{He} \rightarrow p + n + n + \nu_\mu$ process.

| Chiral order | $R = 0.8$ fm | $R = 0.9$ fm | $R = 1.0$ fm | $R = 1.1$ fm | $R = 1.2$ fm | $\delta(\Gamma)$ | $\Delta$ |
|---|---|---|---|---|---|---|---|
| LO | 95 | 99 | 105 | 113 | 120 | 70.0 | 26 |
| NLO | 159 | 157 | 154 | 151 | 148 | 16.1 | 11 |
| N$^2$LO | 161 | 159 | 157 | 154 | 151 | 3.7 | 10 |
| N$^3$LO | 169 | 169 | 171 | 172 | 175 | 0.9 | 6 |
| N$^4$LO | 170 | 169 | 169 | 170 | 173 | 0.2 | 4 |

outgoing neutrino. Results concerning the total capture rate for this process are given in Table II. The LO predictions are far from the other results, but starting from NLO we see a nice convergence of results with respect to the order of the chiral expansion for all the values of $R$. The truncation error $\delta(\Gamma)^{(0)}$ at LO is over two orders of magnitude bigger than the one at N$^4$LO. Its value at N$^4$LO is approx. 0.07% (0.52%) of the capture rate using $R = 0.9$ (1.2) fm. Also in this case the dependence on the cut-off parameter is very weak. The last column in Table II shows the maximal difference between predictions at a given order and for different regulators $R$, $\Delta$, which at N$^4$LO reaches approximately 1.76% for ${}^3\text{He}$ -${}^3\text{H}$ transition. The capture rate obtained for this process with the AV18 $NN$ potential and using the same model of weak current (SNC+RC) equals 1295 s$^{-1}$ and is very close to the chiral value.

For both above-mentioned processes we observe that the cut-off dependence dominates the truncation errors if all five values of the regulator considered here are taken into account, in agreement with the arguments given in Ref. [44]. If one restricts oneself only to the suggested values of the regulator ($R = 0.9$ fm or $R = 1.0$ fm), then the truncation errors and the spread due to the different $R$ are of the same order. We also find, for both capture processes, a small value of $\Delta$ at LO, which seems, however, to us somewhat accidental. It is also interesting to notice that the total capture rates reach their maxima at the same values of the regulator $R = 0.9$ fm and 1.0 fm. Finally, we emphasize that the truncation error $\delta(\Gamma_d)$ at N$^2$LO and higher orders, $\delta(\Gamma_d)^{(\geqslant 3)}$, estimated using Eq. (2.6) does not include information about the actual size of corrections $\Delta\Gamma_d^{(\geqslant 3)}$, which is not available from the incomplete calculations presented here. Also, the uncertainty from the truncation of the chiral expansion of the exchange current operators is not taken into account. Thus, the obtained values of $\delta(\Gamma_d)$ may underestimate the actual theoretical uncertainty at higher orders. In the future, more complete calculations will provide information on the size of contributions beyond N$^2$LO which would allow us to perform a more reliable uncertainty quantification.

In Fig. 12 we show the differential capture rates for the $\mu^- + {}^3\text{He} \rightarrow d + n + \nu_\mu$ (top) and $\mu^- + {}^3\text{He} \rightarrow p + n + n + \nu_\mu$ (bottom) processes as a function of the outgoing neutrino energy $E_\nu$. For both processes the convergence of differential capture rates at $R = 0.9$ fm with respect to the chiral order looks similar. The $NN$ force at LO underestimates the higher-order capture rates by a factor of approximately 3. The NLO and N$^2$LO predictions are close to each other and, finally, the values at N$^3$LO and N$^4$LO are again very similar. The contributions from orders beyond LO play a significant role only above

$E_\nu \approx 80$ MeV in both channels. As in the case of observables for electromagnetic processes presented in the previous sections, the truncation errors are very small at the higher orders, pointing to a full convergence of nuclear forces with respect to the chiral expansion. The cut-off dependence is small and predictions for different regulators overlap, except for the region of the maximal capture rate values. However, even in this case the difference between predictions based on the different $R$ values amounts only to 2.7% (2.3%) at $E_\nu = 95.5$ (90.7) MeV for the two-body (three-body) channel.

The total capture rates for both breakup channels, given in Tables III and IV, show similar behavior as the ones with the ${}^3\text{H}$ in the final state, given in Table II. Both measures of theoretical uncertainties, $\delta(\Gamma)$ and $\Delta$, decreases with the chiral order, and are below 2.5% at N$^4$LO. The values of the capture rates obtained here are in agreement with corresponding results [33] for the AV18 force which are 604 s$^{-1}$ and 169 s$^{-1}$ for the $n+d$ and $n+n+p$ final states, respectively.

## VII. SUMMARY

We applied the recently developed improved chiral $NN$ forces with the semilocal regularization [21,22] to a theoretical description of the deuteron and ${}^3\text{He}$ photodisintegration reactions as well as to the proton-deuteron radiative capture and the muon capture processes on the deuteron and ${}^3\text{He}$. The single nucleon electromagnetic current supplemented by implicit many-body contributions included via the Siegert theorem was used for the processes with real photons. For the muon capture reactions the single nucleon weak current operator was used, supplemented with the dominant, $p^2/M_{\text{nucl}}^2$ relativistic corrections. Despite their simplicity, such models of nuclear currents are sufficient to realize the main goal of this work, which is to verify the usefulness of the locally regularized $NN$ chiral forces in a description of electroweak processes at energies below the pion production threshold.

For all investigated reactions we could confirm the desired behavior of the used $NN$ interaction. Namely, we observed fast convergence of the predictions with respect to the order of the chiral expansion—for all studied observables predictions at N$^4$LO are very close to the ones at N$^3$LO. We also observe very weak dependence of our results on the value of the local regulator $R$. Especially, predictions with the recommended values of regulator [21,22], $R = 0.9$ fm and $R = 1.0$ fm, usually overlap at N$^4$LO. The observed cut-off dependence is much weaker than the one found in Ref. [31] for the older chiral forces [17], which were regularized directly in momentum space using nonlocal regulators. Finally, we estimate the truncation errors coming from neglecting higher-order

contributions. These theoretical uncertainties decrease with the chiral order and are very small beyond N$^2$LO, except for the highest energies studied here. The magnitude of the truncation errors depends on the value of the regulator $R$ and is the biggest for $R = 1.2$ fm. The sizes of the truncation errors at $R = 0.9$ fm and $R = 1.0$ fm are comparable; they are of the same order as the difference between predictions obtained using these regulators. When all the $R$ values are taken into account, the spread of predictions is usually bigger than the truncation error, even for $R = 1.2$ fm. We conclude that in the future only recommended values $R = 0.9$ fm and $R = 1.0$ fm should be used. However, it would be interesting to confirm this observation in nuclear structure calculations.

The quality of the description of the data is rather satisfactory but leaves room for improvement by including contributions from $3N$ forces and many-body parts of the nuclear current operators. Thus, it will be important to identify observables which are sensitive to the details of the dynamical framework. One of the candidate is the deuteron analyzing power $T_{22}$ in the deuteron photodisintegration process. Experimental efforts focused on precise and systematic measurements of such observables would be very important to provide a solid basis for a detailed study of chiral dynamics.

We may thus conclude that the present work confirms the importance of the improved chiral $NN$ potential with the local regularization for few-body investigations in a broad range of energies. Of course we are aware that the final conclusions about the observed patterns can be drawn only when consistent $3N$ force and current operators at all the considered orders of the chiral expansion are included, but the predictions presented here constitute a promising, inescapable first step in this direction.

[1] J. Carlson and R. Schiavilla, Rev. Mod. Phys. **70**, 743 (1998).

[2] S. Bacca and S. Pastore, J. Phys. G: Nucl. Part. Phys. **41**, 123002 (2014).

[3] P. Kammel and K. Kubodera, Annu. Rev. Nucl. Part. Sci. **60**, 327 (2010).

[4] V. D. Efros, W. Leidemann, G. Orlandini, and N. Barnea, J. Phys. G: Nucl. Part. Phys. **34**, R459 (2007).

[5] L. E. Marcucci, M. Piarulli, M. Viviani, L. Girlanda, A. Kievsky, S. Rosati, and R. Schiavilla, Phys. Rev. C **83**, 014002 (2011).

[6] L. E. Marcucci, A. Kievsky, S. Rosati, R. Schiavilla, and M. Viviani, Phys. Rev. Lett. **108**, 052502 (2012).

[7] R. Machleidt and D. R. Entem, Phys. Rep. **503**, 1 (2011).

[8] E. Epelbaum, H.-W. Hammer, and Ulf-G. Meißner, Rev. Mod. Phys. **81**, 1773 (2009).

[9] E. Epelbaum, A. Nogga, W. Glockle, H. Kamada, Ulf-G. Meißner, and H. Witala, Phys. Rev. C **66**, 064001 (2002).

[10] E. Epelbaum, A. Nogga, W. Glöckle, H. Kamada, Ulf-G. Meißner, and H. Witała, Eur. Phys. J. A **15**, 543 (2002).

[11] E. Epelbaum, A. Nogga, H. Witała, H. Kamada, W. Glöckle, and Ulf-G. Meißner, Eur. Phys. J. A **17**, 415 (2003).

[12] W. Glöckle, E. Epelbaum, H. Kamada, Ulf-G. Meißner, A. Nogga, and H. Witała, Eur. Phys. J. A **19**, 159 (2004).

[13] A. Kievsky, M. Viviani, L. Girlanda, and L. E. Marcucci, Phys. Rev. C **81**, 044003 (2010).

[14] M. Viviani, A. Baroni, L. Girlanda, A. Kievsky, L. E. Marcucci, and R. Schiavilla, Phys. Rev. C **89**, 064004 (2014).

[15] J. Carlson, S. Gandolfi, F. Pederiva, S. C. Pieper, R. Schiavilla, K. E. Schmidt, and R. B. Wiringa, Rev. Mod. Phys. **87**, 1067 (2015), and references therein.

[16] K. Hebeler, J. D. Holt, J. Menéndez, and A. Schwenk, Annu. Rev. Nucl. Part. Sci. **65**, 457 (2015).

[17] E. Epelbaum, W. Glöckle, and Ulf-G. Meißner, Nucl. Phys. A **747**, 362 (2005).

[18] H. Witała, J. Golak, R. Skibiński, and K. Topolnicki, J. Phys. G: Nucl. Part. Phys. **41**, 094011 (2014).

[19] J. Golak *et al.*, Eur. Phys. J. A **50**, 177 (2014).

[20] R. Skibiński, J. Golak, K. Topolnicki, H. Witała, E. Epelbaum, W. Glöckle, H. Krebs, A. Nogga, and H. Kamada, Phys. Rev. C **84**, 054005 (2011).

[21] E. Epelbaum, H. Krebs, and Ulf-G. Meißner, Eur. Phys. J. A **51**, 53 (2015).

[22] E. Epelbaum, H. Krebs, and U. G. Meißner, Phys. Rev. Lett. **115**, 122301 (2015).

[23] S. Binder *et al.*, Phys. Rev. C **93**, 044002 (2016).

[24] T.-S. Park, D.-P. Min, and M. Rho, Nucl. Phys. A **596**, 515 (1996).

[25] S. Pastore, R. Schiavilla, and J. L. Goity, Phys. Rev. C **78**, 064002 (2008).

[26] A. Baroni, L. Girlanda, S. Pastore, R. Schiavilla, and M. Viviani, Phys. Rev. C **93**, 015501 (2016).

[27] S. Kolling, E. Epelbaum, H. Krebs, and U. G. Meißner, Phys. Rev. C **80**, 045502 (2009).

[28] S. Kolling, E. Epelbaum, H. Krebs, and U. G. Meißner, Phys. Rev. C **84**, 054008 (2011).

[29] D. Rozpędzik, J. Golak, S. Kölling, E. Epelbaum, R. Skibiński, H. Witała, and H. Krebs, Phys. Rev. C **83**, 064004 (2011).

[30] R. Skibiński, J. Golak, D. Rozpiędzik, K. Topolnicki, and H. Witała, Acta Phys. Polon. **B46**, 159 (2015).

[31] R. Skibiński, J. Golak, H. Witała, W. Glöckle, A. Nogga, and E. Epelbaum, Acta Phys. Polon. **B37**, 2905 (2006).

[32] G. Shen, L. E. Marcucci, J. Carlson, S. Gandolfi, and R. Schiavilla, Phys. Rev. C **86**, 035503 (2012).

[33] J. Golak, R. Skibinski, H. Witala, K. Topolnicki, A. E. Elmeshneb, H. Kamada, A. Nogga, and L. E. Marcucci, Phys. Rev. C **90**, 024001 (2014).

[34] J. Golak, H. Kamada, H. Witala, W. Glockle, J. Kuros, R. Skibinski, V. V. Kotlyar, K. Sagara, and H. Akiyoshi, Phys. Rev. C **62**, 054005 (2000).

[35] R. Skibiński, J. Golak, H. Kamada, H. Witała, W. Glöckle, and A. Nogga, Phys. Rev. C **67**, 054001 (2003).

[36] J. Golak, R. Skibiński, H. Witała, W. Glöckle, A. Nogga, and H. Kamada, Phys. Rep. **415**, 89 (2005).

[37] R. Skibiński, J. Golak, H. Witała, W. Glöckle, and A. Nogga, Eur. Phys. J. A **24**, 31 (2005).

[38] H. Arenhövel, Z. Phys. A **302**, 25 (1981).

[39] H. Arenhövel, Lect. Notes Phys. **426**, 1 (1994).

[40] H. Arenhövel and M. Sanzone, Few-Body Syst. Suppl. **3**, 1 (1991).

[41] J. D. Walecka, *Theoretical Nuclear and Subnuclear Physics* (Oxford University Press, New York, 1995).

[42] W. Glöckle, H. Witała, D. Hüber, H. Kamada, and J. Golak, Phys. Rep. **274**, 107 (1996).

[43] A. Nogga, D. Hüber, H. Kamada, and W. Glöckle, Phys. Lett. B **409**, 19 (1997).

[44] E. Epelbaum *et al.* (unpublished).

[45] R. B. Wiringa, V. G. J. Stoks, and R. Schiavilla, Phys. Rev. C **51**, 38 (1995).

[46] R. Moreh, T. J. Kennett, and W. V. Prestwich, Phys. Rev. C **39**, 1247 (1989).

[47] D. M. Skopik, Y. M. Shin, M. C. Phenneger, and J. J. Murphy, Phys. Rev. C **9**, 531 (1974).

[48] M. Bosman, A. Bol, J. F. Gilot, P. Leleux, P. Lipnik, and P. Macq, Phys. Lett. B **82**, 212 (1979).

[49] Y. Birenbaum, S. Kahane, and R. Moreh, Phys. Rev. C **32**, 1825 (1985).

[50] R. Bernabei *et al.*, Phys. Rev. Lett. **57**, 1542 (1986).

[51] S. Ying, E. M. Henley, and G. A. Miller, Phys. Rev. C **38**, 1584 (1988), and references therein.

[52] I. A. Rachek *et al.*, Phys. Rev. Lett. **98**, 182303 (2007).

[53] S. I. Mishnev *et al.*, Phys. Lett. B **302**, 23 (1993).

[54] F. Ritz, H. Arenhövel, and T. Wilbois, Few-Body Syst. **24**, 123 (1998).

[55] W. Tornow, N. G. Czakon, C. R. Howell, A. Hutcheson, J. H. Kelley, V. N. Litvinenko, S. F. Mikhailov, I. V. Pinayev, G. J. Weisel, and H. Witała, Phys. Lett. B **574**, 8 (2003).

[56] M. P. DePascale *et al.*, Phys. Rev. C **32**, 1830 (1985).

[57] I. E. Vnukov *et al.*, Pisma Zh. Eksp. Teor. Fiz. **43**, 510 (1986) [Sov. Phys. JETP Lett. **43**, 659 (1986)].

[58] V. P. Barannik *et al.*, Sov. J. Nucl. Phys. **38**, 667 (1983).

[59] G. Mitev, P. Colby, N. R. Roberson, H. R. Weller, and D. R. Tilley, Phys. Rev. C **34**, 389 (1986).

[60] B. D. Belt, C. R. Bingham, M. L. Halbert, and A. van der Woude, Phys. Rev. Lett. **24**, 1120 (1970).

[61] W. K. Pitts *et al.*, Phys. Rev. C **37**, 1 (1988).

[62] K. Sagara, H. Kiyoshi, S. Ueno, N. Nishimori, A. Motoshima, R. Koyasako, K. Nakashima, T. Fujita, K. Maeda, H. Nakamura, and T. Nakashima, AIP Conf. Proc. **334**, 467 (1995).

[63] H. Akiyoshi, Ph.D. thesis, Kyushu University, 1997.

[64] R. Skibiński, J. Golak, H. Witała, W. Glöckle, H. Kamada, and A. Nogga, Phys. Rev. C **67**, 054002 (2003).